Received June 25, 2019, accepted July 15, 2019, date of publication July 22, 2019, date of current version August 27, 2019.

Digital Object Identifier 10.1109/ACCESS.2019.2930298

Broadbeam Cylindrical Dielectric Resonator Antenna

SYEDA H. H. MASHHADI[1], YONG-CHANG JIAO[2], (Senior Member, IEEE), AND JINGDONG CHEN[1], (Senior Member, IEEE)

[1]Center of Intelligent Acoustics and Immersive Communications, Northwestern Polytechnical University, Xi'an 710072, China
[2]National Key Laboratory of Antennas and Microwave Technology, Xidian University, Xi'an 710071, China

Corresponding author: Syeda H. H. Mashhadi (hiba.mashhadi@mail.nwpu.edu.cn)

ABSTRACT A novel widebeam aperture-coupled cylindrical dielectric resonator antenna is proposed, which consists of multi-layered cylindrical ceramic disks joined together to achieve the required height. The proposed antenna is fed by wide aperture slot, which, along with optimum dielectric resonator height, excites fundamental and high order hybrid modes inside the DR to achieve wide beamwidths in the two principal planes simultaneously. Then, a new frequency, which is called the limited frequency and denoted as f_L, is defined. Based on f_L, dimensions of the wide slot are determined. Finally, the antenna is manufactured and measured. Its operating frequency band ranges from 5.49 GHz to 7.2 GHz. The antenna yields broadbeam in the frequency band from 6.1 to 6.7 GHz and achieves a 3-dB beamwidth from 124° to 149° in the E-plane and from 112° to 126° in the H-plane.

INDEX TERMS Broadbeam dielectric resonator antennas, cylindrical dielectric resonator antennas, higher order hybrid modes.

I. INTRODUCTION

Wide angular coverage and stable radiation patterns (no multi-lobes in the main beam) are two very critical antenna characteristics required for a vast range of applications [1], [2]. Achieving 3-dB beamwidths of more than 120° in both working planes simultaneously, however, is a challenging task and an emerging research topic [3]. While they are widely used, microstrip patch antennas (MPAs) can only achieve 3-dB beamwidths of 110° and 70° in the E- and H-planes, respectively, which are insufficient for applications or systems requiring wide 3-dB beamwidths [4]. There have been a great number of works published in the literature presenting procedures for broadening the 3-dB beamwidth for MPAs. In [5], Duan *et al*. proposed an antenna based on a two-layer stacked electromagnetic coupling microstrip patch antenna. This technique was shown to be able to yield stable 60° half power beamwidth (HPBW) in the E- and H-planes. A dual beam and wide beam antenna was proposed by Dadgarpour *et al.* [6]. The dielectric constant of the antenna substrate is artificially modified using arrays of metamaterial inclusions yielding a 60° 3-dB beamwidth. A rectangular patch on a composite substrate was demonstrated to have 75% increase in the H-plane 3-dB beamwidth and 10% increase in the E-plane 3-dB beamwidth [7]. The aforementioned works show that a fair amount of attention has been paid to developing methods and procedures to enhance 3-dB beamwidths of MPAs.

In contrast, dielectric resonator antennas (DRAs) have not received much attention in this particular regard. One of the very initial efforts for improving the 3-dB beamwidth using dielectrics within microstrip patch antenna construction was presented by Haidan in [4]. Afterwards, a design with improved 3-dB beamwidth was patented by Chang and Kiang in 2008, in which carved ground plane was used to widen the beamwidth of a rectangular DRA to yield 120° 3-dB beamwidths in both planes [8]. Techniques like patch loaded DRA [9] and reduced ground plane [10] have so far been used to widen the 3-dB beamwidths of a DRA. Detailed numerical study and evaluation of modes inside the cylindrical DRA (CDRA) can be found in [11], [12]. Knowledge of broadside modes and their respective modal-fields inside the DR is generally an initial step towards the task of beamwidth broadening. In accordance with the IEEE standard [13], the hybrid modes in a dielectric resonator are denoted by HEM_{mnp}, where the first, second, and third subscripts specify the nature of the azimuthal, radial, and axial variations, respectively. There is a lot of work reported on

The associate editor coordinating the review of this manuscript and approving it for publication was Kwok L. Chung.

the design of CDRAs with broadside *HEM* modes excited. For instance, HEM_{111} and HEM_{113} have been excited simultaneously, employing an aperture feed and a metallic strip at the edge of the cylindrical dielectric resonator (CDR) is used for dual band operation in [14]. Guha *et. al* in [17] propose to excite a broadside higher order hybrid mode ($HEM_{12\delta}$) for high gain radiation pattern in CDRAs. In [18], [19], Guha *et. al* propose $HEM_{12\delta}$ as a new mode and presents a technique to excite this mode using a nonresonant microstrip patch (NMP). This mode ($HEM_{12\delta}$), though is a broadside mode, yields narrow beamwidths in both the planes which are estimated to be less than 80° in both principal planes because it yields high gain. Gain and radiation pattern beamwidths are known to have an inverse relation. Similarly, in [20], a CDR has been used as a feed. This too yields a broadside radiation pattern but with an estimated beamwidth of less than 70° in both planes. This mode inherently yields a broad H-plane pattern compared to E-plane. In [21], fundamental hybrid mode is excited to investigate the coupling characteristics of aperture slot feed with a thick ground plane. In [22], input impedance of an HEM_{111} aperture coupled CDRA has been investigated for different slot dimensions. In [24], a new mode has been excited in a CDRA to achieve wide beam radiation pattern in H-plane only. It yields a strawberry shaped radiation pattern with half power beamwidth of 130° in H-plane only. Most of those works either employ complex feeding mechanisms or present complicated antenna structures to achieve performance enhancement or to investigate a certain parameter with respect to the other. There are only a very small number of works found in regard to enhancing the 3-dB beamwidth of DRAs, which still focus in one plane.

In this paper, design of an aperture fed CDRA yielding wide 3-dB beamwidths in both principal planes, simultaneously is presented. Furthermore, a method is proposed to identify the band of frequencies which are critical for broadbeam operation. Results show that a CDRA can yield widebeam radiation patterns in a frequency band ranging from the resonance frequency of fundamental mode to that of next azimuthal higher order hybrid mode. By using a wide slot only, fundamental mode HEM_{111} and higher order hybrid mode HEM_{113} are excited inside the CDR. No additional feeding mechanism to improve the coupling of these two modes simultaneously is required as is demonstrated by Fang and Leung [14]. The 3-dB beamwidths of more than 120° are achieved in both planes. This work can serve as a basis for broadbeam DRA design. The potential applications include, but not limited to, automotive radars for auto cruise control [25], GPS, telemetry, which require wide angular coverage. Since the proposed methodology has been validated in C ($4 - 8$ GHz) band, a few potential applications in this particular range are C-band weather radar [26], antenna for beacon missiles and target drones, satellite communication, wireless LAN, electric toll collection systems (ETC) and vehicle-to-roadside communication. The latter two are radio-frequency identification (RFID) services and require short range, low to medium gain antennas. The proposed relations of antenna dimensions with λ_l hold true at all the frequency bands with the current feeding mechanism, which is simple and cost effective from fabrication point of view. Therefore, the process of frequency-translation of proposed antenna at any desired range is quite straight forward.

The remainder of this paper is organized as follows. Section II describes configuration of the proposed antenna. The working principle and mode analysis are presented in Section III. Section IV presents the parametric analysis as well as the guidelines for the antenna design. Section V describes the implementation of the proposed methodology on an aperture coupled CDRA design already presented in [21] in order to improve its 3-dB beamwidth in two planes. Simulations and experiments are carried out and the results are summarized and analyzed in Section VI. Finally, important conclusions are drawn in Section VII.

II. ANTENNA CONFIGURATION

In this section, a broadbeam aperture coupled CDRA is presented, which is illustrated in Fig. 1. The proposed DRA is fed by 50-Ω microstrip feed line. The fields are coupled into the DR through a wide slot with length $sl = 0.208\lambda_l$ and width $sw = 0.125\lambda_l$ (where λ_l is wavelength of the frequency, for a specific DR height at which the first 3 modes have same resonance). Size of the substrate is $Lgx \times Lgy$, where the ground plane length (Lgx) and breadth (Lgy) are both equal to $1.27\lambda_l$. It has been shown in [16]–[20] that in low profile CDRs (with the height-to-radius ratio less than 1) HEM_{111} can be successfully excited, where the CDRs are made with a certain ceramic board cut into a cylinder. However, the height of the proposed wide beam CDR is greater than the heights or the thicknesses of many off-the-shelf ceramic boards. Therefore, in order to keep the design low-cost and easy to fabricate, the CDR is constructed by joining several low profile (2 mm thick) ceramic disks together to attain the required height.

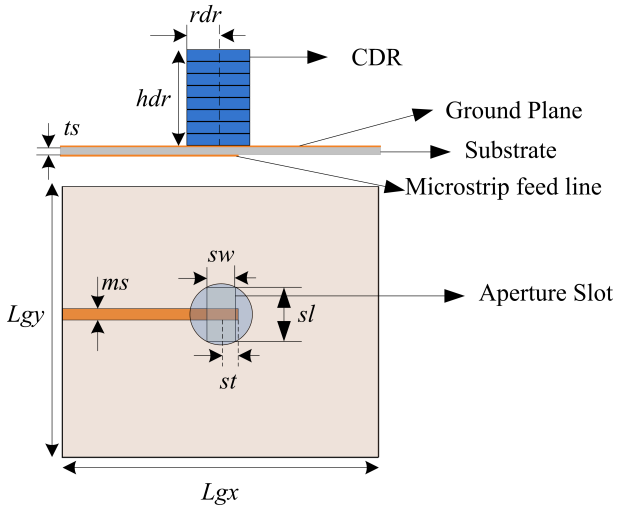

FIGURE 1. The proposed wide beam CDRA fed by a wide slot on the substrate with relative permittivity $\epsilon_s = 4.4$, DR relative permittivity $\epsilon_{dr} = 9.8$, $Lgx = Lgy = 61$ mm, $ts = 1.5$ mm, $ms = 3$ mm, $sw = 6$ mm, and $sl = 10$ mm.

TABLE 1. Parameters of proposed broadbeam CDRA.

Parameter name	Parameter	Value
DR Radius	rdr	6 mm
DR Height	hdr	16 mm
Substrate Thickness	ts	1.5 mm
Slot Width	sw	6 mm
Slot Length	sl	10 mm
Microstrip feed width	ms	3 mm
GP side length	$Lgx = Lgy$	61 mm

The dielectric constant ϵ_{dr} used for CDR in antenna is chosen to be 9.8. Table 1 enlists optimized parameter values of the antenna.

III. WORKING PRINCIPLE

In this section, vector field distributions of hybrid modes inside the CDR are studied in detail. Hybrid modes are critical for broadbeam operation because experiments and simulations show that HEM_{111} in CDRA yields broad E-plane and narrow H-plane 3 dB beamwidths while HEM_{113} yields wider H-plane and narrow E-plane beamwidths. It is imperative to mention here that in CDRAs HEM_{112} mode cannot be used since it is canceled by the ground plane effect [14]. Therefore, it is conjectured that in frequency band between Mode-I and Mode-III resonance frequencies, a CDRA must yield uniform and wide beamwidth radiation patterns in both the E- and H-plane simultaneously. Furthermore, it is well known that higher order hybrid mode can be excited inside a CDR with height-to-radius ratio of more than 3. The initial dimensions of CDR and HEM_{111} resonance frequency are calculated using the following equations [15]:

$$F = \frac{30(k_o a)}{2\pi a} \tag{1}$$

$$k_o a = \frac{1.6 + 0.513x + 1.392x^2 - 0.575x^3 + 0.088x^4}{\epsilon_{dr}^{0.42}} \tag{2}$$

where $x = a/2h$. The calculated Mode-I resonance frequency with the given parameters in this work is 5.29 GHz for $a = rdr = 6$ mm and $h = hdr = 16$ mm.

Next, the high frequency structure simulator (HFSS) software package eigen mode solver is used to verify the natural resonant behavior of isolated CDR. This model consists of CDR placed upon an infinite ground plane. There is a good agreement between Mode-I resonance calculated using Equation 1 and 2 and that found using HFSS eigen mode solver, which is 5.4 GHz. Figure 2 shows the electric and magnetic field vector distributions at 5.4 GHz, which is Mode-I frequency. The electric and magnetic vector field distributions are used to identify the slot orientation for maximum coupling of fields into the CDR. To excite Mode-I, a source which in this case is a slot, should be placed at a strong magnetic field to get good coupling. However, in order to keep the design costs reasonable, the CDR is constructed using 2-mm thick ceramic disks which causes a slight shift in mode resonances. This shift in frequencies may be caused by the adhesive used to attach each CDR layer and air-gaps introduced between consecutive layers. However, the preferred

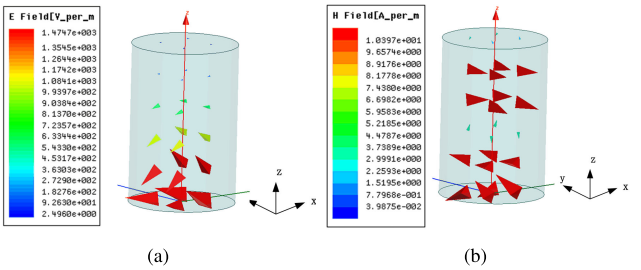

FIGURE 2. Vector field distribution of isolated CDRA residing on infinite ground plane at 5.4 GHz (Mode-I resonance): (a) electric field vector plot, and (b) magnetic field vector plot.

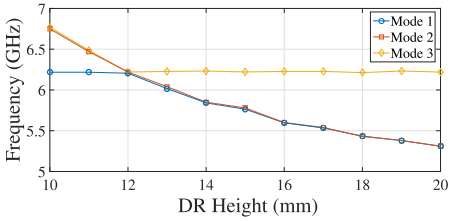

FIGURE 3. Frequency versus DR height.

orientation of aperture slot remains the same for stacked and one piece CDR.

Now the relation between CDR height, hdr and mode resonances is studied. Figure 3 plots mode resonance frequencies of the stacked isolated CDR for changing CDR heights. When the height is varied, CDR radius is kept constant. Each curve plotted in Fig. 3 corresponds to a specific mode and consequently a specific vector field distribution. Following facts are validated upon analyzing Fig. 3; First is that Mode-II cannot be excited since the curve corresponding to Mode-II is only following the other two curves. Second is that at a specific height, $hdr = 12$ mm, Mode-I and Mode-III have the same resonance frequency of 6.2 GHz. This frequency and the DR height it corresponds to is of much significance; So, we name this frequency as the *limited frequency*, denoted by f_{L}, at and above which the antenna yields broad beam radiation patterns in two planes simultaneously. The DR height corresponding to $f_{\text{L}} = 6.2$ GHz is $0.25\lambda_l = 12$ mm. For CDR height values greater than $0.25\lambda_l$ the antenna H-plane 3-dB beamwidth increases considerably along with the increase of the E-plane 3-dB beamwidth.

To further analyze how 3-dB beamwidths are effected by mode vector field distributions inside the CDR, they are analyzed in detail at selected frequencies. Figure 4 illustrates

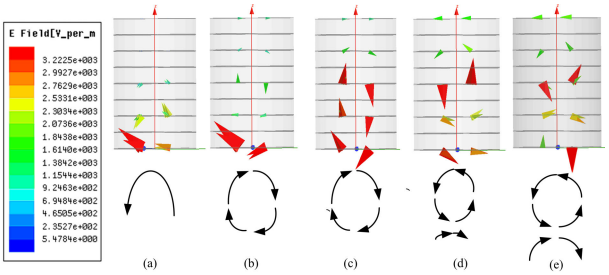

FIGURE 4. Vector field distributions at (a) 5.4 GHz, (b) 5.8 GHz, (c) 6.2 GHz, and (d) 6.6 (e) 7.1 GHz GHz.

the mode vector field distributions inside the CDR at 5.4 GHz, 5.8 GHz, 6.2 GHz, 6.6 GHz, and 7.1 GHz. At this point it is important to recall from Fig. 3 that at the DR height of 16 mm, the mode resonances in order of mode number are 5.4 GHz (Mode-I) and 6.2 GHz (Mode-III); but when the CDR is placed on a finite ground plane and is fed with an aperture slot, the mode resonance frequencies shift towards slightly higher frequencies. This shift occurs because HFSS eigen mode solver setup does not take into consideration the effects of finite ground plane and excitation source. Therefore, it can be concluded that Mode-I has shifted from 5.4 GHz to 5.8 GHz, but the vector field distribution of Mode-I can be observed at both frequencies as is clear from Fig. 4. Vector field distributions at both of those frequencies are hence important to be studied, which are shown in Fig. 4. The use of wide slot also widens resonance bandwidth of each mode. Before explaining the mode vector field distributions, it is important to mention that since azimuthal hybrid modes are under consideration, the number of half e-field cycles along the azimuthal direction defines mode order, which is the third subscript p of the mode nomenclature HEM_{mnp}. At 5.4 GHz as shown in Fig. 4a, the mode is identified as the fundamental hybrid mode, i.e., HEM_{111}, owing to the presence of one half-cycle of the e-field inside the CDR. However, as it can be seen from Fig. 4b and Fig. 4c that from 5.8 GHz to 6.2 GHz, Mode-I like vector field distributions may be observed. At 5.8 GHz, the antenna has a radiation pattern corresponding to the mode with broad E-plane 3-dB beamwidth (103.5°) and narrow H-plane 3-dB beamwidth (97.53°). Conventional low profile CDRAs have a broad E-plane beamwidth (between 110° and 125°). However, the H-plane beamwidth is narrow (generally between 80° and 90°). According to the plot in Fig. 3, 6.2 GHz is Mode-III resonance, but it also tends to shift due to finite ground plane to 6.6 GHz. So, fields at these two frequencies are also very important to be studied. In Fig. 4d, at 6.6 GHz there are three e-field half cycles or alternatively it can be stated that one complete e-field cycle as well as the introduction of one half e-field cycle. This indicates that at frequencies after 6.6 GHz Mode-III is expected to couple strongly. Frequencies above 6.6 GHz are included in Mode-III resonance bandwidth. Fields at 6.2 GHz and 6.6 GHz are also important to be studied. Finally, in Fig. 4e the mode is clearly identified as HEM_{113}, owing to the presence of three half e-field cycles or one and a half e-field cycles. Furthermore, for frequencies starting from 6.2 GHz to 6.7 GHz, it can also be observed from the vector field distributions at each frequency that with increasing frequency the influence of Mode-I becomes lesser and that of Mode-III becomes stronger. These two modes have been simultaneously excited by a wide aperture slot.

In order to emanate a clear idea of relation between vector field distributions of specific modes and 3 dB beamwidths in two planes, E- and H-plane radiation patterns at each of these frequencies at which vector field distributions are shown in Fig. 4 are presented in Fig. 5. It can be seen that at 5.4 GHz, Fig. 5a, the E- and H-plane radiation patterns

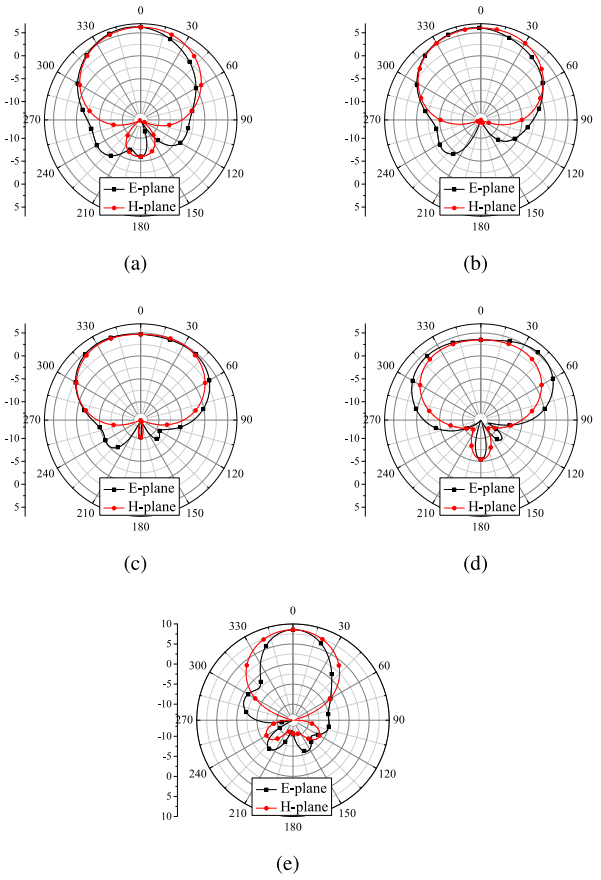

FIGURE 5. E- and H-plane radiation patterns at (a) 5.4 GHz (b) 5.8 GHz (c) 6.2 GHz (d) 6.6 GHz (e) 7.1 GHz.

yield narrow 3-dB beamwidths of 93° and 81°, respectively. This frequency corresponds to Mode-I as can be confirmed from Fig. 3 and Fig 4. At 5.8 GHz, Fig. 5b, E- and H-plane 3 dB beamwidths are 103.5° and 97.53°, respectively. From Fig. 4b, it has already been established that the vector field distribution at 5.8 GHz is of Mode-I. Here, it is concluded that Mode-I alone cannot be responsible for widebeam radiation patterns in two planes simultaneously. Moving further, it is clear that at 6.2 GHz, the E- and H-plane 3-dB beamwidths are wide simultaneously. Referring to Fig. 4c, vector field distribution at 6.2 GHz appears to be Mode-I like fields but not exactly Mode-I. At 6.6 GHz, Fig. 5d, the radiation patterns are quite wide in both the planes with E- and H-plane 3 dB beamwidths being 138° and 128°, respectively. Finally at 7.1 GHz, Fig. 5e, the E- and H-plane radiation patterns yield narrow 3-dB beamwidths. At this frequency, Mode-III vector field distribution can be clearly observed from Fig. 4e and are identified as HEM_{113}. Figure 4 and Fig. 5 clearly show the relation between modal fields and 3-dB beamwidths. Vector field distributions of Mode-I and Mode-III do not yield wide beamwidths in both planes. It is the band of frequencies between these two modes in which wide beamwidths are achieved in two planes simultaneously. Table 2 enlists 3-dB beamwidths at the above mentioned frequencies.

Comparison between the 3-dB beamwidths of the CDRAs designed using the proposed technique and the ones

TABLE 2. The 3-dB beamwidths at various mode frequencies.

Frequency (GHz)	E-plane HPBW	H-plane HPBW	Mode
5.4 GHz	93°	81°	Mode-I
5.8 GHz	103.5°	97.53°	Mode-I-like
6.2 GHz	124°	115°	Mode-II-like
6.6 GHz	138°	128°	Mode-III
7.1 GHz	43°	64°	Mode-III

developed in [9], [14], [20]–[24] is presented in Table 3. It is imperative to mention here that due to lack of literature on beamwidth enhancement of DRAs, such designs or researches which excite broadside modes in their proposed DRAs are chosen and their beamwidths are either estimated or the designs are implemented to get a clear estimate of beamwidths. How to determine the antenna parameters will be discussed in the next section.

IV. PARAMETRIC ANALYSIS

In this section, the influence of some important parameters on the reflection coefficients, the *xoz*-plane 3-dB beamwidths, and the *yoz*-plane 3-dB beamwidths are investigated. When one parameter is studied, the others are kept constant. The results should provide useful guidelines for practical design.

A. PARAMETRIC ANALYSIS FOR CDRA RADIATION APERTURE

First, the effect of CDRA radiation aperture on beamwidths is investigated. The radiation aperture of CDRA includes the dielectric resonator (DR) and ground plane over which the DR resides. Therefore, the DR height, *hdr*, the ground plane x-axis oriented length (*Lgx*) and the y-axis oriented length (*Lgy*) are varied to study their impact on *xoz* and *yoz* beamwidths. Figure 6 plots *xoz* and *yoz* 3-dB beamwidths for various DR height. It is clear that as the DR height is reduced, the beamwidth becomes narrow. For smaller DR heights like $hdr = 4$ mm, Mode-III cannot be excited at all. As the height increases, azimuthal higher order mode i.e. HEM_{113} (Mode-III) is also excited. In addition to DR height, slot dimensions play a role in widening the reso-

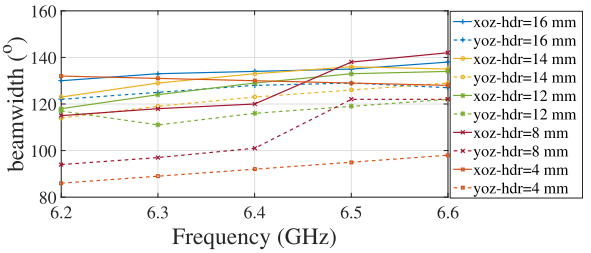

FIGURE 6. Beamwidth versus DR height *hdr*.

nance bandwidth of Mode-I and Mode-III. Consequently both modes are excited simultaneously. Figure 7 plots the reflection coefficients for different values of ratio hdr/rdr. When the ratio is equal to or greater than 2, the antenna begins to yield wide 3-dB beamwidths. As the DR height increases, influence of higher order mode increases. The aim is to identify a DR height such that Mode-I and Mode-III are optimally excited simultaneously. When this is done, it becomes clear that the transition between these two modes is the band of frequencies where broad beamwidths in both planes are achieved. In Fig. 7, for hdr/rdr ratio equal to 2.33, 2.66 and 3, the reflection coefficient curve is almost flat in the frequency band ranging from 6.0 to 6.6 GHz. Also, it can be observed that in the same band of frequencies, Mode-I (HEM_{111}) and Mode-III (HEM_{113}) are simultaneously excited. Having identified the 3 important hdr/rdr ratios or in other words the optimum DR heights, which cause two modes to be excited simultaneously, Table 4 can be referred to for finding the ratio hdr/rdr that yields widest 3-dB beamwidths. Table 4 shows the effect of the ratio height-to-radius on *xoz* and *yoz* plane 3-dB beamwidths and gives an important insight into the selection criteria of the optimum hdr/rdr. When the hdr/rdr ratios are greater than 2, the 3-dB beamwidths in both planes are optimized, uniform and wide.

Figures 8 and 9 show varying ground plane dimensions versus *xoz* and *yoz* 3-dB beamwidths. It is clear from Fig. 8 that when the x-axis oriented ground plane length $Lgx = 1.27\lambda_l = 61$ mm, 3-dB beamwidths are maximum. Similar is the case when $Lgy = 61$ mm as shown in Fig. 9. When the y-oriented ground plane dimension, $Lgy = 1.27\lambda_l$,

TABLE 3. Comparison of Estimated 3-dB Beamwidths of DRAs in the literature with the proposed widebeam CDRA.

Ref. No.	Authors	E-plane HPBW	H-plane HPBW	Height/radius	ε_{dr}	Mode
[9]	K. Y. Hui *et al.*	120°	57°	NA	NA	NA
[14]	X. S. Fang *et al.*	71° 105°	82° 88°	>2	9.4	$HEM_{11\delta}$ HEM_{113}
[16]	X. Di *et al.*	92°	91°	1.0	10	$HEM_{11\delta}$
[20]	P. Gupta *et al.*	128°	98°	0.95	9.8	$HEM_{11\delta}$
[21]	Y.-X Guo *et al.*	84°	82°	2	8.9	$HEM_{11\delta}$
[22]	G. P. Junker *et al.*	86°	83°	0.8	37	$HEM_{11\delta}$
[23]	K. W. Leung *et al.*	148°	75°	1.0	10	$HEM_{11\delta}$
[24]	D. Guha *et al.*	<85°	130°	1.0	10	New mode
This work	Mashhadi *et al.*	138°	122°	3.3	9.8	HEM_{111} HEM_{113}

NA means "not available"

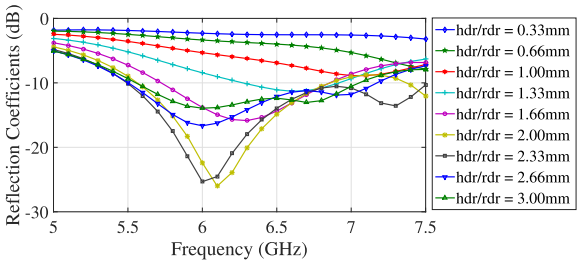

FIGURE 7. Reflection coefficient versus *hdr*/*rdr* ratio.

TABLE 4. 3-dB Beamwidths of the proposed CDRA at 6.2 GHz for different *hdr*/*rdr* ratio.

hdr/rdr	e-plane HPBW	h-plane HPBW
$2/6 = 0.33$	132°	81°
$4/6 = 0.66$	131°	84°
$6/6 = 1.00$	123°	87°
$8/6 = 1.33$	117°	93°
$10/6 = 1.66$	113°	96°
$12/6 = 2.00$	119°	106°
$14/6 = 2.33$	124°	114°
$16/6 = 2.66$	129°	124°
$18/6 = 3.00$	125°	121°

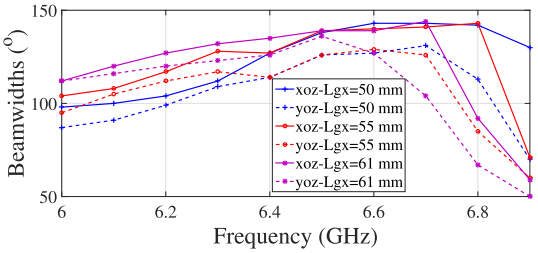

FIGURE 8. Beamwidth versus x-axis ground plane length *Lgx*.

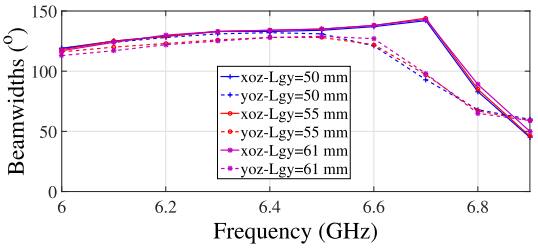

FIGURE 9. Beamwidth versus y-axis ground plane length *Lgy*.

the *xoz* and *yoz* 3-dB beamwidths are maximum. The most important fact to be noted here is that *Lgx* has more pronounced effect on *yoz* 3 dB beamwidth compared to *Lgy*. But the most optimized *yoz* beamwidth is achieved when *Lgx* and *Lgy* both are equal.

B. PARAMETRIC ANALYSIS FOR FEEDING SLOT DIMENSIONS

Besides the DR height, another important parameter that plays a vital role in exciting Mode-I and Mode-III simultaneously are the slot dimensions. Figures 10 and 11 show the effects of changing slot length and slot width, respectively on −10 dB reflection coefficients. In both figures, red colored plot shows the most optimum dimensions which are 10 mm slot length and 6 mm slot width. Although in Fig. 10 the

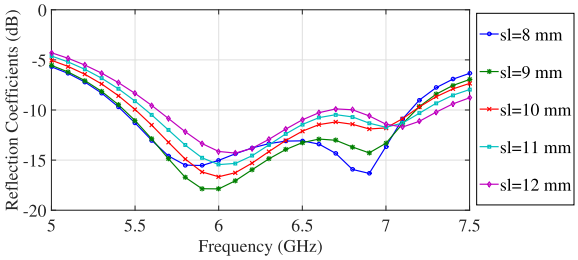

FIGURE 10. Reflection coefficient versus slot length.

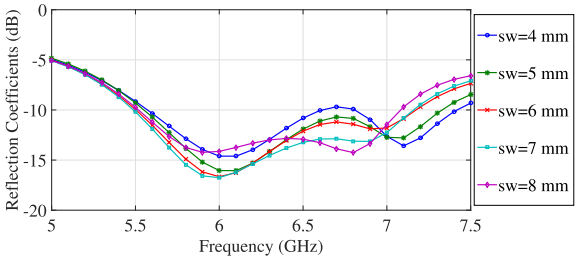

FIGURE 11. Reflection coefficient versus slot width.

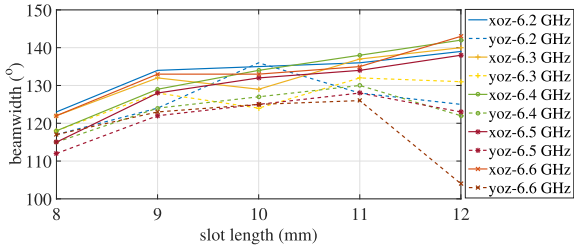

FIGURE 12. Beamwidth versus slot length.

optimal value for the reflection coefficient is when the slot length is 8 mm and in Fig. 11 the optimal value also happens when the slot width is 8 mm; but these two dimensions are not chosen, the underlying reason is evident from Figs. 12 and 13, which plot the *xoz* and *yoz* beamwidths with varying slot lengths and slot widths, respectively. In both the figures, the lines for the *yoz* beamwidth plot are dotted in order to differentiate from those for the *xoz* beamwidth plot. From Fig. 12, one can see that when the slot length is between 9 mm and 11 mm, the *xoz* and *yoz* beamwidth values are close to each other, which indicates that they are uniform, so a slot length value is chosen from this range. Similarly, in Fig. 13 when the slot width is between 5 mm and 7 mm, the *xoz* and *yoz* 3-dB beamwidths are widest, therefore, slot width value is chosen from this range.

Based on these results, the initial steps for the broadbeam CDRA design are summarized as follows. The first step,

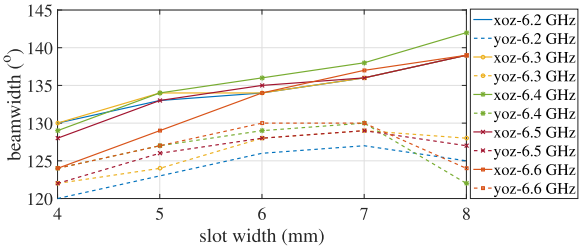

FIGURE 13. Beamwidth versus slot width.

which is also the most important step, is the selection of a ceramic material with relative permittivity between 5 and 12. Simulation results indicate that ceramics with relative permittivity higher than 12 is not so good for the proposed method. The second step is to set the hdr/rdr ratio of the CDR equal to or greater than 2.5. The limited frequency, i.e., f_{L}, should be identified using the HFSS eigen mode solver where it is defined as the frequency at which higher order modes tend to have the same resonance as the fundamental mode. The third step is to place the DR on a slot with slot length of $0.208\lambda_l$ and slot width of $0.125\lambda_l$. This would result in a wide slot, which also causes high back radiation but it is still 20 dB less than the main beam as will become evident from the radiation pattern results presented in Section VI. The optimal ground plane size is $Lgx \times Lgy$, where $Lgx = Lgy = 1.27\lambda_l$. The stub length st is $0.08\lambda_l$ where the stub length is the length starting from center of the slot to the open end of the microstrip feed line.

V. METHODOLOGY VALIDATION

In order to validate the proposed method and to study the antenna dimensions in terms of λ_l, it is implemented on an aperture coupled CDRA presented in [21]. The referenced CDRA dielectric resonator (DR) height, b is 10.35 mm, DR radius, a is 10.9 mm with a dielectric constant of 9.2 and a microwave substrate thickness of $h = 1.59$ mm and dielectric constant, $\epsilon_{rs} = 2.33$. The microstrip feed line width, W_f of 5 mm. The slot dimensions, $W \times L$ are 1 mm $\times$ 12 mm. The steps defined in the previous section are followed in order to enhance the beamwidth of the CDRA. Step 1 is to choose DR dielectric constant between 5 and 12. The implemented antenna has ϵ_{dr} less than 12. The hdr/rdr ratio of the CDR is changed from 0.95 to 3. Using HFSS eigen mode solver, f_{L} is found out to be 3.5 GHz and modal resonances of Mode-I and Mode-III equal to 3.1 GHz and 3.5 GHz, respectively. This provides with a clear range of frequencies within which the widebeam radiation pattern yielding frequencies are found. Next step is to change the slot length, slot width and stub length according to the relations given in the previous section. Originally the CDRA was excited with a narrow aperture slot, which yields reflection coefficient such that it has a narrow notch at one particular frequency. The changed wide slot antenna, however is relatively wideband with Mode-I and Mode-III excited simultaneously. Figure 14a and Fig. 14b plot the E- and H-plane radiation pattern of the original antenna as well as the radiation pattern for the modified broadbeam CDRA, respectively. The results validate the proposed method.

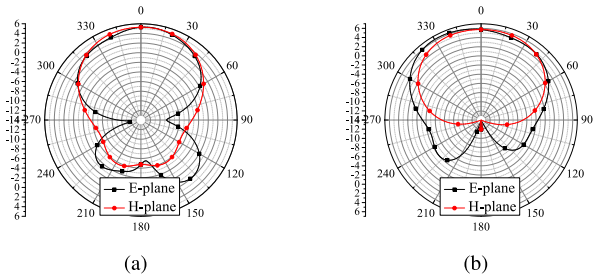

FIGURE 14. Radiation patterns of a CDRA at 3.2 GHz [21]: (a) E-plane and H-plane 3-dB beamwidths; 92° and 91° (b) E-plane and H-plane 3-dB beamwidths; 128° and 119°.

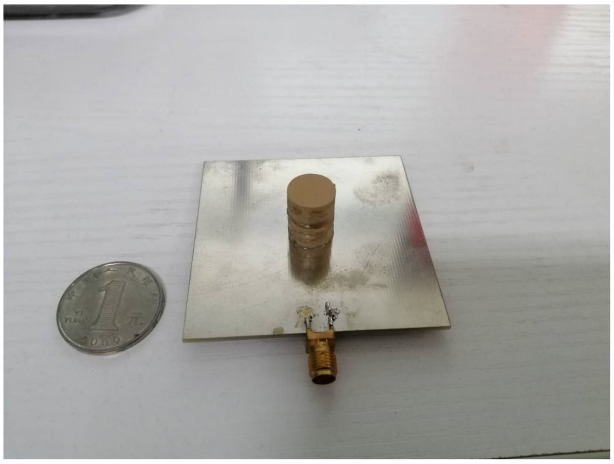

FIGURE 15. Photograph of the fabricated broadbeam CDRA.

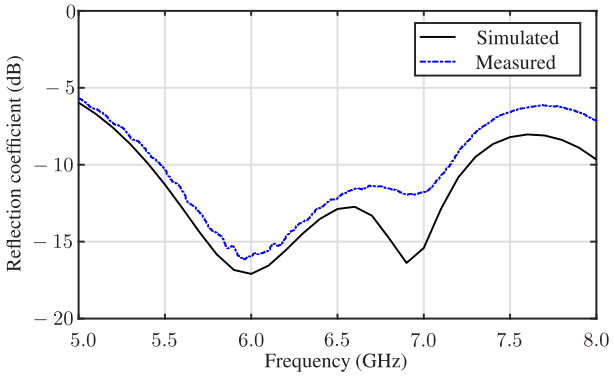

FIGURE 16. Measured and simulated reflection coefficients.

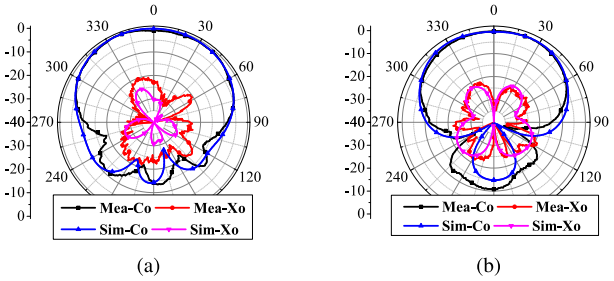

FIGURE 17. Radiation patterns at 6.2 GHz: (a) E-plane, 3-dB beamwidth = 128° (b) H-plane, 3-dB beamwidth = 123°.

VI. ANTENNA PERFORMANCE

To validate the proposed design technique, a prototype is fabricated and measured, as shown in Fig. 15. Both the simulated and measured reflection coefficients of the antenna are plotted in Fig. 16. The differences between the measured and simulated results are mainly caused by the rough outer surfaces of the fabricated DR and air gaps introduced by the adhesive in between consecutive CDR disks. Figure 17 plots the measured and simulated E- and H-plane radiation patterns at 6.2 GHz for proposed broadbeam CDRA. In Figs. 18 and 19, the radiation patterns at 5.8 GHz and 7.1 GHz, respectively, are plotted for both planes. One can clearly see that the

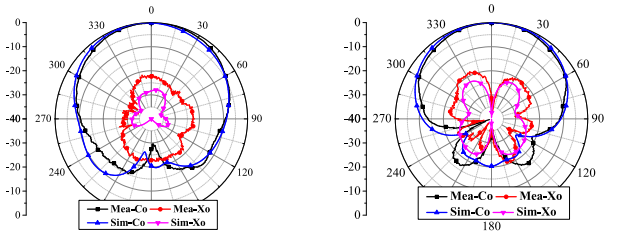

FIGURE 18. Radiation patterns at 5.8 GHz: (a) E-plane, 3-dB beamwidth = 97° (b) H-plane, 3-dB beamwidth = 103°.

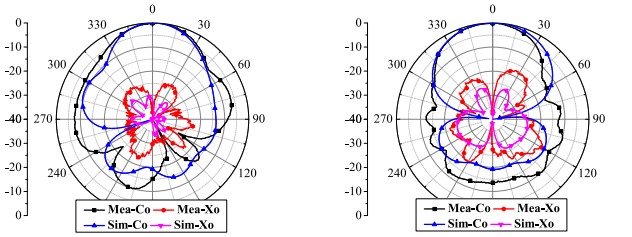

FIGURE 19. Radiation patterns at 7.1 GHz: (a) E-plane, 3-dB beamwidth = 24° (b) H-plane, 3-dB beamwidth = 64°.

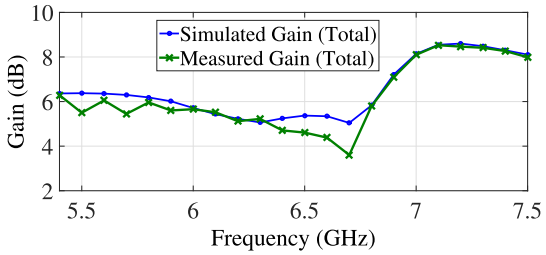

FIGURE 20. Measured and simulated gain of the proposed broadbeam CDRA.

beamwidths are narrower for the frequencies 5.8 GHz and 7.1 GHz. The measured patterns agree quite well with the simulated patterns. The 3-dB beamwidths in both planes are broad and uniform. Isolation between co-to-cross polarized radiations is approximately 20 − 22 dB, which is satisfactory for practical applications. Simulated and measured reflection coefficients of the proposed antennas are obtained using ANSYS HFSS and the Agilent Technologies E8363B PNA, respectively. The radiation patterns are measured in an anechoic chamber using the vector network analyzer Anritsu MS4644A. In Fig. 20, the simulated and measured gain of the proposed broadbeam CDRA are plotted for the entire operating frequency band. In Fig. 21, the simulated and measured *xoz* and *yoz* 3-dB beamwidths are plotted. In frequency range of 6.0 GHz to 6.6 GHz, the 3-dB beamwidths are clearly higher for both planes compared to the those at the rest of the band.

VII. CONCLUSION

A widebeam CDRA is presented in this paper and a design method is proposed. The antenna is fed by wide slot, which is shown to be able to excite HEM_{111} and HEM_{113} simultaneously to yield broad 3-dB beamwidths in both the E- and H-planes when the DR height-to-radius ratio is

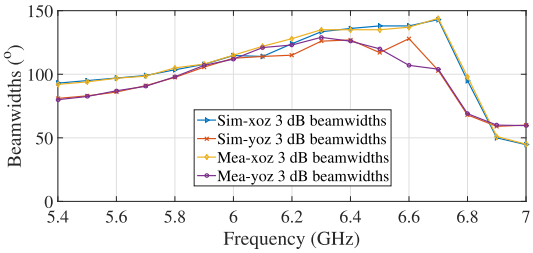

FIGURE 21. Measured and simulated 3-dB beamwidth of the proposed broadbeam CDRA.

between 2 and 3. A new frequency f_L is defined based on which optimum dimensions for broadbeam CDRA are determined. The antenna yields broadbeam radiation patterns in the frequency band from 6.1 GHz to 6.7 GHz and 3-dB beamwidths of more than 120° in both the E- and H-planes in this band. Its operating frequency band is from 5.49 GHz to 7.2 GHz. The proposed antenna is also low cost owing to its construction using thin ceramic disks, which are stacked and glued together to attain the required height. The antenna gain ranges from 5.2 dB to 5.4 dB in the broadbeam band of frequencies.

ACKNOWLEDGMENT

The authors would like to thank Dr. Huan Zhang, Dr. Chaoyi Cui, Mr. Hongwei Yu, Mr. Yixuan Zhang, and Mr. Zhendong Wang from Xidian University and Kangkang Han from Northwestern Polytechnic University, Xi'an, China for their time and guidance in antenna fabrication and measurement.

REFERENCES

[1] S. Chattopadhyay, J. Y. Siddiqui, and D. Guha, "Rectangular microstrip patch on a composite dielectric substrate for high-gain wide-beam radiation patterns," *IEEE Trans. Antennas Propag.*, vol. 57, no. 10, pp. 3325–3328, Oct. 2009.

[2] R. Patel and K. J. Han, "Utilization of higher-mode resonance in broadening the E-plane HPBW of printed antenna for automotive radar application," in *Proc. Int. Workshop Antenna Technol. (iWAT)*, Mar. 2015, pp. 330–332.

[3] R. Mittra, R. Yang, M. Itoh, and M. Arakana, "Microstrip patch antennas for GPS applications," in *Proc. IEEE Antennas Propag. Soc. Int. Symp.*, Ann Arbor, MI, USA, vol. 3, Jun./Jul. 1993, pp. 1478–1481.

[4] H. Haidan, "A novel wide beam circular polarization antenna - microstrip-dielectric antenna," in *Proc. 3rd Int. Conf. Microw. Millim. Wave Technol. (ICMMT)*, Beijing, China, Aug. 2002, pp. 381–384.

[5] Z. S. Duan, S. B. Qu, Y. Wu, and J. Q. Zhang, "Wide bandwidth and broad beamwidth microstrip patch antenna," *Electron. Lett.*, vol. 45, no. 5, pp. 249–250, Feb. 2009.

[6] A. Dadgarpour, B. Zarghooni, B. S. Virdee, and T. A. Denidni, "Single end-fire antenna for dual-beam and broad beamwidth operation at 60 GHz by artificially modifying the permittivity of the antenna substrate," *IEEE Trans. Antennas Propag.*, vol. 64, no. 9, pp. 4068–4073, Sep. 2016.

[7] A. A. Kishk, M. R. Zunoubi, and D. Kajfez, "A numerical study of a dielectric disk antenna above grounded dielectric substrate," *IEEE Trans. Antennas Propag.*, vol. 41, no. 6, pp. 813–821, Jun. 1993.

[8] T.-H. Chang and J.-F. Kiang,"Dielectric resonator antenna with bending metallic planes," U.S. Patent, 10 102 739 A1, 2008.

[9] K. Y. Hui and K. M. Luk, "A patch loaded dielectric resonator antenna," in *Proc. IEEE Region Conf.(TENCON)*, Melbourne, QLD, Australia, Nov. 2005, pp. 1–4.

[10] Y. He, W. Wang, and X. Du, "A wide-band wide-beam dielectric resonator antenna," in *Proc. IEEE Conf. Antenna Meas. Appl. (CAMA)*, Tsukuba, Japan, Dec. 2017, pp. 210–212.

[11] D. Kajfez, A. W. Glisson, and J. James, "Evaluation of modes in dielectric resonators using a surface integral equation formulation," in *IEEE MTT-S Int. Microw. Symp. Dig.*, Boston, MA, USA, pp. 409–411, May/Jun. 1983.
[12] D. Kajfez, A. W. Glisson, and J. James, "Computed modal field distributions for isolated dielectric resonators," in *IEEE MTT-S Inter. Microw. Symp. Dig.*, May/Jun. 1984, pp. 193–195.
[13] A. G. Jensen *et al.*, "IRE standards on antennas and waveguides: Definitions of terms, 1953," *Proc. IRE*, vol. 41, no. 12, pp. 1721–1728, Dec. 1953.
[14] X. S. Fang and K. W. Leung, "Linear-/circular-polarization designs of dual-/wide-band cylindrical dielectric resonator antennas," *IEEE Trans. Antennas Propag.*, vol. 60, no. 6, pp. 2662–2671, Jun. 2012.
[15] K. M. Luk and K. W. Leung, *Dielectric Resonator Antennas*. London, U.K.: Research Studies Press,2011.
[16] X. Di, A. W. Glisson, and K. A. Michalski, "Analysis of a dielectric resonator antenna in a cylindrical conducting cavity: HEM modes," *IEE Proc.-Microw., Antennas Propag.*, vol. 141, no. 1, pp. 8–14, Feb. 1994.
[17] D. Guha, A. Banerjee, C. Kumar, and Y. M. M. Antar, "Higher order mode excitation for high-gain broadside radiation from cylindrical dielectric resonator antennas," *IEEE Trans. Antennas Propag.*, vol. 60, no. 1, pp. 71–77, Jan. 2012.
[18] D. Guha, A. Banerjee, C. Kumar, and Y. M. M. Antar, "New technique to excite higher-order radiating mode in a cylindrical dielectric resonator antenna," *IEEE Antennas Wireless Propag. Lett.*, vol. 13, pp. 15–18, 2013.
[19] D. Guha, P. Gupta, and C. Kumar, "Dual band cylindrical dielectric resonator antenna employing $HEM_{11\delta}$ and $HEM_{12\delta}$ modes excited by new composite aperture," *IEEE Trans. Antennas Propag.*, vol. 63, no. 1, pp. 433–438, Jan. 2015.
[20] P. Gupta, D. Guha, and C. Kumar, "Dielectric resonator working as feed as well as antenna: New concept for dual-mode dual-band improved design," *IEEE Trans. Antennas Propag.*, vol. 64, no. 4, pp. 1497–1502, Apr. 2016.
[21] Y.-X. Guo, K.-M. Luk, and K.-W. Leung, "Characteristics of aperture-coupled cylindrical dielectric resonator antennas on a thick ground plane," *IEE Proc.-Microw., Antennas Propag.*, vol. 146, no. 6, pp. 439–442, Dec. 1999.
[22] G. P. Junker, A. A. Kishk, and A. W. Glisson, "Input impedance of dielectric resonator antennas excited by a coaxial probe," *IEEE Trans. Antennas Propag.*, vol. 42, no. 7, pp. 960–966, Jul. 1994.
[23] K. W. Leung and S. K. Mok, "Circularly polarised dielectric resonator antenna excited by perturbed annular slot with backing cavity," *Electron. Lett.*, vol. 37, no. 15, pp. 934–936, Jul. 2001.
[24] D. Guha, P. Gupta, and C. Kumar, "New mode in dielectric resonator antenna with strawberry shaped radiations covering a wide beamwidth," in *Proc. IEEE Antennas Propag. Soc. Int. Symp. (APSURSI)*, Jul. 2013, pp. 1912–1913.
[25] W. Menzel and A. Moebius, "Antenna concepts for millimeter-wave automotive radar sensors," *Proc. IEEE*, vol. 100, no. 7, pp. 2372–2379, Jul. 2012.
[26] A. M. Flashy and A. V. Shanthi, "Microstrip circular antenna array design for radar applications," in *Proc. Int. Conf. Inf. Commun. Embedded Syst. (ICICES)*, Chennai, India, Feb. 2014, pp. 1–5.

SYEDA H. H. MASHHADI received the B.E. degree in telecommunication (electrical) engineering from the Military College of Signals, National University of Sciences and Technology (NUST), Rawalpindi, Pakistan, in 2007, and the M.S. degree in communication engineering from the University of Manchester, U.K., in 2009. She is currently pursuing the Ph.D. degree in information and communication engineering with Northwestern Polytechnical University (NPU), Xi'an, China.

Her previous research has been on broadband monopole blade/fin antenna design for air borne applications, broadband VHF high power sleeved dipole designs, bi-conical high power broadband antennas, and textile dielectric resonator antennas (DRAs) for body area networks (BAN). Her current research interests include investigation of several shapes of dielectric resonator antennas for achieving wide beam radiation patterns and substrate integrated waveguide (SIW) fed widebeam DRAs and arrays. She received the Agilent's Best Student Award from the University of Manchester, for outstanding performance.

YONG-CHANG JIAO (SM'13) received the B.S. degree in mathematics from Shanxi University, China, in 1984, and the M.S. degree in applied mathematics and the Ph.D. degree in electrical engineering from Xidian University, Xi'an, China, in 1987 and 1990, respectively.

In 1990, he joined the Institute of Antennas and EM scattering, Xidian University, where he is currently a Professor. From March to June 1996, he was a JSPS Visiting Priority-Area Research Fellow with the University of Tsukuba, Japan. From October 1997 to January 1998 and from July 1999 to April 2000, he was a Research Associate with the Chinese University of Hong Kong, Hong Kong. From March to September 2002, he was a Research Fellow with the City University of Hong Kong, Hong Kong. He has authored or coauthored more than 250 papers in technical journals and conference proceedings. His papers have been cited more than 2500 times with an H-index of 28 (source: ISI Web of Science). His current research interests include antenna designs and computational electromagnetics.

Dr. Jiao is also a Senior Member of the Chinese Institute of Electronics (CIE) and a member of the Antenna Committee of CIE. He was elected a Deputy to the 9th, 10th, and 11th Shaanxi Provincial People's Congress. He was also a member of the Standing Committee of the 10th and 11th Shaanxi Provincial People's Congress.

JINGDONG CHEN (M'99–SM'09) received the Ph.D. degree in pattern recognition and intelligence control from the Chinese Academy of Sciences, in 1998.

From 1998 to 1999, he was with the ATR Interpreting Telecommunications Research Laboratories, Kyoto, Japan, where he conducted research on speech synthesis, speech analysis, and objective measurements for evaluating speech synthesis. He then joined the Griffith University, Brisbane, Australia, where he is involved in research on robust speech recognition and signal processing. From 2000 to 2001, he was with the ATR Spoken Language Translation Research Laboratories on robust speech recognition and speech enhancement. From 2001 to 2009, he was a Member of Technical Staff with Bell Laboratories, Murray Hill, New Jersey, working on acoustic signal processing for telecommunications. He subsequently joined WeVoice Inc. in New Jersey, serving as the Chief Scientist. He is currently a Professor with the Northwestern Polytechnical University, Xi'an, China. His research interests include acoustic signal processing, adaptive signal processing, speech enhancement, adaptive noise/echo control, microphone array signal processing, signal separation, and speech communication.

Dr. Chen was a Technical Committee (TC) Member of the IEEE Signal Processing Society (SPS) TC on Audio and Electroacoustics, from 2007 to 2009. He is currently a member of the IEEE SPS TC on Audio and Acoustic Signal Processing, and a member of the Editorial Advisory Board of the *Open Signal Processing Journal*. He received the 2008 Best Paper Award from the IEEE Signal Processing Society (with Benesty, Huang, and Doclo), the Best Paper Award from the IEEE Workshop on Applications of Signal Processing to Audio and Acoustics, in 2011 (with Benesty), and the Bell Labs Role Model Teamwork Award twice, in 2009 and 2007, respectively, and the Young Author Best Paper Award from the 5th National Conference on Man-Machine Speech Communications, in 1998. He is the coauthor of a paper for which his Ph.D. student, C. Pan received the IEEE R10 (Asia-Pacific Region) Distinguished Student Paper Award (First Prize), in 2016. He was a recipient of the Japan Trust International Research Grant from the Japan Key Technology Center, in 1998, and the "Distinguished Young Scientists Fund" from the National Natural Science Foundation of China (NSFC), in 2014. He was the General Co-Chair of ACM WUWNET 2018 and IWAENC 2016, the Technical Program Chair of IEEE TENCON 2013, a Technical Program Co-Chair of IEEE WASPAA 2009, IEEE ChinaSIP 2014, IEEE ICSPCC 2014, and IEEE ICSPCC 2015, and helped organize many other conferences. He served as an Associate Editor for the IEEE TRANSACTIONS ON AUDIO, SPEECH, AND LANGUAGE PROCESSING, from 2008 to 2014.